High-performance ammonia-selective MFI nanosheet membranes

Xuekui Duan, ^a Donghun Kim, ^{ab} Katabathini Narasimharao ^c Shaeel Al-Thabaiti, ^c and Michael Tsapatsis *ade

Abstract

Nanosheet-based MFI membranes, known to be highly selective for hydrocarbon isomer separations, exhibit NH₃/N₂ mixture separation factor of 2,236 with NH₃ permeance of 1.1×10⁻⁶ mol/(m².s.Pa), and NH₃/H₂ separation factor of 307 with NH₃ permeance of 2.3×10⁻⁶ mol/(m².s.Pa) at room temperature. Consistent with a competitive sorption-based separation, lower operating temperatures and higher pressures result in increased separation factor. At 323K, with an equimolar mixed feed of NH₃/N₂, the fluxes and separation factors at 3 and 7 bar are: 0.13 mol/(m²·s) and 191, and 0.26 mol/(m²·s) and 220, respectively. This performance compares favorably with that of other membranes and suggests that MFI membranes can be used in separation and purification processes involving mixtures of NH₃/N₂/H₂ encountered in ammonia synthesis and utilization. The membranes also exhibit high performance for the separation of ethane, *n*-propane and *n*-butane from H₂.

Keywords: MFI nanosheet, MFI Membrane, Ammonia separation, Sorption-based separation

^a Department of Chemical Engineering and Materials Science, University of Minnesota Twin Cities, 421 Washington Ave SE, Minneapolis, MN 55455, USA, Email: tsapa001@umn.edu

^b School of Chemical Engineering, Chonnam National University, Gwangju 61186, Republic of Korea.

^c Department of Chemistry, Faculty of Science King Abdulaziz University (KAU), P.O. Box 80203 Jeddah 21589, Saudi Arabia.

^d Department of Chemical and Biomolecular Engineering & Institute for NanoBioTechnology, Johns Hopkins University, 3400 N. Charles Street, Baltimore, MD 21218, USA.

^e Applied Physics Laboratory, Johns Hopkins University, 11100 Johns Hopkins Road, Laurel, MD 20723, USA.

Introduction

Various types of membranes, including liquid (for high temperature operation) $^{1-3}$ and polymeric $^{4-11}$ membranes have been explored as potential contributors to energy efficient processes for ammonia separation. However, liquid membranes suffer from structural instabilities, and polymeric membranes from the decline of performance at industrially relevant high-pressure and temperature conditions. Alternatively, silica $^{12;13}$ and zeolite 12 membranes have also been proposed for this application, but the reported combinations of permeances and selectivities are not sufficient for practical applications. In ref. 12 , the highest zeolite membrane separation factor obtained for NH₃/H₂ separation was ca. 10, with a NH₃ permeance of 2.1×10^{-7} mol/(m².s.Pa) at 80 °C. Silica membranes showed a higher permeance (7.6×10⁻⁷ mol/(m².s.Pa)) but even lower selectivity (ca. 7). Kanezashi et al. 13 reported a silica membrane with a NH₃ permeance of 1.0×10^{-7} mol/(m².s.Pa) and a NH₃/H₂ separation factor of ca. 30 at 50 °C.

Recently, by using directly synthesized high-aspect-ratio zeolite MFI nanosheets, ultra-selective MFI membranes with unprecedented permeances and separation factors for *para*-xylene/*ortho*-xylene were obtained using secondary growth ^{14,15}. Herein, we report that these thin, oriented, and large-grain zeolite MFI membranes exhibit outstanding performance for the separation of ammonia from hydrogen and nitrogen. The membranes are also evaluated for the separation of hydrocarbons from hydrogen.

Material and methods

<u>Direct synthesis of MFI nanosheets:</u> The MFI nanosheets were prepared by a synthesis procedure reported previously ^{S1}, using seeded growth templated by a certain structure directing agent (SDA): bis-1,5(tripropyl ammonium) pentamethylene diiodide (dC5). In brief, first, MFI nanocrystals were prepared as seeds for the growth of nanosheets, using a sol with molar composition of 10SiO₂:2.4TPAOH:0.87NaOH:114H₂O. A precursor sol with a composition of 80TEOS:3.75dC5:20 KOH:9500 H₂O was hydrolyzed and mixed with the MFI nanocrystal suspension at 1000:1 silica molar ratio of precursor sol to nanocrystal suspension. The mixture was then transferred into a Teflon-lined stainless steel autoclave and hydrothermally treated statically at 140 °C for 4 days.

Preparation of porous sintered silica fiber (SSF) supports: Sintered silica fiber (SSF) supports were prepared by following the same procedures reported earlier ^{S2}. First, commercially available silica fibers, referred to as quartz fibers, were crushed and pressed followed by sintering at 1100 °C and for 3 hours and polishing using CarbiMetTM SiC abrasive paper (600 grit/P1200). Then, 500 nm Stöber silica spheres were rubbed manually on the top surface followed by sintering at 1100 °C for 3 hours. This rubbing and sintering process was repeated up to 5-8 times until the surface was fully covered by the Stöber silica spheres. Finally, a top 50 nm Stöber silica layer was rubbed on the surface and fixed on the surface by sintering at 450 °C for 6 hours. It serves as the silica source to form continuous and inter-grown films by the gel-free secondary growth method ^{S3}.

Fabrication of MFI membranes: Membrane fabrication was performed following the exact procedures reported earlier ^{S4}. Briefly, the synthesized MFI nanosheets were purified using centrifugation and dispersed in DI water containing 5 vol% ethanol. To form a thin layer of nanosheet coating on the porous SSF support as seeds, the floating particle method was used ^{S4}. The support was placed in a home-made TeflonTM trough. After filling the trough with DI water, the suspension was transferred to the air-water interface using a micropipette, forming a uniform layer of MFI nanosheets. Then, by lowering the water level below the support, the MFI nanosheet layer was deposited on the support surface, to obtain a uniform layer of nanosheet coating. The coated support was then dried and calcined at 400 °C for 6 hours. This coatings process was repeated twice to ensure high surface coverage by the nanosheets. Finally, the seeded support was treated by the gel-free secondary growth ^{S3} at 180 °C for 4 days using an impregnating TPAOH aqueous solution (0.025M TPAOH) to obtain a well-intergrown membrane, which was calcined at 450 °C for 6 hours.

<u>Characterization:</u> X-ray diffraction (XRD) patterns were obtained using a Panalytical X'Pert Pro diffractometer with Cu Kα radiation at 45 kV and 40 mA. SEM measurements were performed on a

FEG-SEM (Hitachi SU8230) at 5 kV. The cross-sectional FIB-SEM images of the membrane were obtained by FEI Helios NanoLab G4 dual-beam focused ion beam (FIB).

Permeation test: The membranes were tested under different feed pressures. The hydrocarbon/ H_2 atmospheric feed pressure tests were performed in the Wicke–Kallenbach mode (70 mL/min hydrocarbon/hydrogen mixture feed with permeate side purged with 30 mL/min sweep gas (Ar)). For membrane tests at higher feed pressures, no sweep gas was used. The feed pressure was regulated by a pressure regulator and measured by a pressure gauge. The permeate side was kept at atmospheric pressure. After maintaining the membrane for ca. 20 hours at each condition to ensure steady state stable operation, the concentrations of feed and permeate streams were determined by GC with a thermal conductivity detector (GC/TCD), equipped with a packed-bed column (Chromosorb PAW, Agilent). Ar was used as carrier gas for the GC. At each permeation condition, the analysis was repeated at least three times. The membrane separation performance is typically assessed with permeance and separation factor. The permeance is the flux normalized by the partial pressure gradient across the membrane. The separation factor is defined as the composition ratio of components A and B in the permeate mixture relative to the composition ratio of A and B in the retentate mixture, i.e. $SF(AB) = [X_A/X_B]_{permeate} / [X_A/X_B]_{retentate}$.

Results and discussion

A well-intergrown zeolite MFI membrane, as confirmed by a high separation performance for an equimolar binary mixture of para-/ortho-xylene (i.e., a para-xylene permeance of 2.3×10⁻⁷ mol/(m².s.Pa) and a separation factor of >3000 at 150 °C and 1 kPa equimolar para-/ortho-xylene feed), is used to evaluate the performance for the separation of ammonia and hydrogen or nitrogen. Typical surface morphology and cross-sectional FIB-SEM image of the fabricated MFI membrane are shown in Figure S1, and are consistent with those reported in previous report ¹⁵. The same membrane is used for all reported NH₃/H₂ and NH₃/N₂ experiments herein. Figure 1a (and Table S1) shows the NH₃/H₂ binary mixture separation performance at different temperatures. Permeation measurements are performed using an equimolar NH₃/H₂ mixture feed at 3 bar while the permeate is kept at 1 bar. No sweep gas is used in the permeate side in an effort to mimic conditions that would be encountered in an actual separation process. At room temperature, the membrane exhibits a NH₃/H₂ mixture separation factor of ca. 307 with a NH₃ permeance of 2.3×10⁻⁶ mol/(m².s.Pa), which corresponds to a flux of 0.09 mol/(m².s). This indicates that the membrane achieves a 99.6% NH₃ purity in the permeate from the equimolar mixture of NH₃/H₂ feed. The mixture separation factor, at the same feed and permeate pressures, drops drastically when the temperature increases; it is 23.8 at 50 °C and 3.8 at 100 °C. A similar trend for the separation performance is observed for the NH₃/N₂ separation, as shown in Figure 1b and Table S2. The membrane exhibits a NH_3/N_2 mixture separation factor of ca. 2,236 at room temperature with a NH_3 permeance of 1.1×10^{-6} mol/(m².s.Pa), which corresponds to a flux of 0.07 mol/(m².s). The separation factor drops to 191 at 50 °C and 16 at 100 °C. Figure 1e and Figure 1f compare the MFI membrane separation factor and NH₃ flux with literature reported values for NH_3/N_2 and NH_3/H_2 separation at/near room temperature, respectively. Compared with other membranes, the nanosheet-based MFI membrane exhibits a desirable combination of high flux and separation factor. This opens the possibility for industrial NH₃/H₂/N₂ separation

The high membrane separation factor towards ammonia at room temperature can be explained by the preferred adsorption of ammonia over hydrogen or nitrogen. Based on reported adsorption isotherms of NH₃ in pure silica MFI ¹⁶, at 298 K and 3 bar (1.5 bar NH₃), MFI pores are occupied by NH₃ at a loading of 2.6 mol/kg, which is high when compared with the saturation capacity (ca. 4.3 mol/kg). The preferred adsorption of NH₃ in the zeolite pores can hinder or block the flow of hydrogen or nitrogen, thus resulting in a high membrane separation factor towards ammonia. At higher temperatures, the loading of NH₃ in MFI pores is decreased, resulting in a drastic decrease of the membrane separation factor.

MFI pores is decreased, resulting in a drastic decrease of the membrane separation factor.

Using the NH₃ isotherms reported in ref. ¹⁶ and the NH₃ diffusivities reported by Jobic et al. ¹⁷, which range from 6×10⁻¹¹ to 10⁻⁹ m²/s and are reported to increase with loading due to the presence of immobile and mobile adsorbed NH₃, we can estimate (see) that the expected NH₃ flux at 25 °C with a feed pressure of 1.5 bar and permeate pressure of 1 bar ranges from 0.03 to 0.47 mol/(m².s), which is in good agreement

with the experimentally obtained values of 0.07 to 0.09 mol/(m².s).

We have also tested the effect of pressure on the membrane separation performance using NH₃/N₂ equimolar feed. Figures 1c and 1d (Table S2) show NH₃ fluxes at various feed pressures and 1 bar undiluted permeate at fixed temperature of 50 and 100 °C, respectively. By increasing the feed pressure, NH₃ flux and separation factor increase. The increase in flux at high feed pressures is due to the higher driving force at higher transmembrane pressure differences. The increase in membrane separation factor

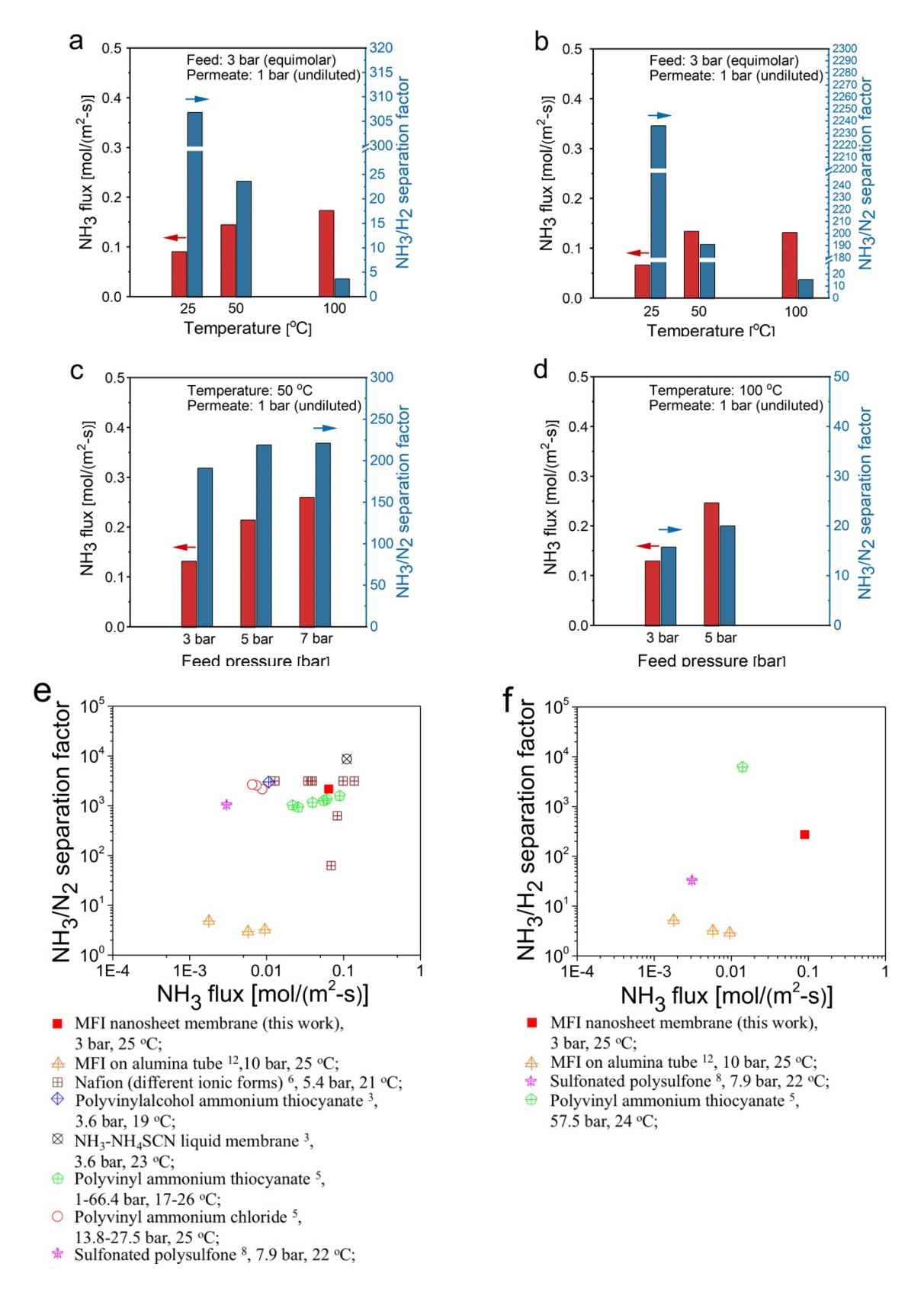


Figure 1. Membrane separation performance for NH_3/H_2 and NH_3/N_2 . NH_3 fluxes and mixture separation factors obtained using an equimolar NH_3/H_2 (a) and NH_3/N_2 (b) feed at different temperatures (25, 50 and 100 °C) with fixed feed pressure of 3 bar. NH_3/N_2 separation non-diluted permeate); permeate pressure: 1 bar. Comparison of NH_3/N_2 (e) and NH_3/H_2 (f) separation performance (separation factor vs. NH_3 flux) for the membranes reported here and representative data from the literature (ref. 3,5,6,8,12 , see Appendix S1-S4).

can also be explained by the fractional loading of NH₃ in zeolite pores; at higher pressures, higher NH₃ loadings diminish the transport of nitrogen. At this time, we could not investigate higher pressures due to safety considerations in our system. It would be important to determine the separation performance of MFI membranes at or near the NH₃ saturation loading at the corresponding testing temperatures. Higher

pressures and temperatures than the ones investigated here will be of interest for certain practical applications ¹⁸.

The competitive adsorption separation mechanism responsible for the observed NH₃/N₂ and NH₃/H₂ selectivity, is well established for the separation of larger and heavier hydrocarbons from lighter gases like , nitrogen ²² and methane ²³⁻²⁷. Although the novel finding of this report is the aforementioned NH₃ selective performance, we also report on the separation of H₂ and hydrocarbon mixtures, which we can compare with the corresponding reported performance of other MFI membranes. Figure 2 shows the membrane separation performance of binary (Figure 2a) and ternary (Figure 2b) H₂ and various hydrocarbon (i.e. ethane, n-propane and n-butane) mixtures at room temperature and atmospheric pressure on both feed and permeate sides (Ar is used as permeate sweep gas). The data are listed in Table S3 and S4. The membrane rejects hydrogen in the presence of hydrocarbons at room temperature. With decreasing hydrocarbon molecular weight, the permeance increases slightly. As expected, n-butane results in a higher $H_2/hydrocarbon$ separation factor (ca. 60) compared to H_2/n -propane (ca. 40) and H_2/e thane (ca. 6). This finding agrees with the reported trend of light alkanes adsorption isotherms in silicalite-1 ²⁸ and reported permeation data ¹⁹⁻²⁷ (Appendix S5). As the hydrocarbon loading increases with pressure, the separation factor is also expected to increase. Indeed, Figure 2c shows an increase of separation factor with increasing feed pressure for H_2/n -butane mixture at low *n*-butane concentration (2 mol%). Figure 2d shows membrane permeation tests with equimolar H₂ and n-propane binary mixture at room temperature and higher feed pressures. By increasing the feed pressure, the membrane shows improved separation factor from ca. 30 to 80.

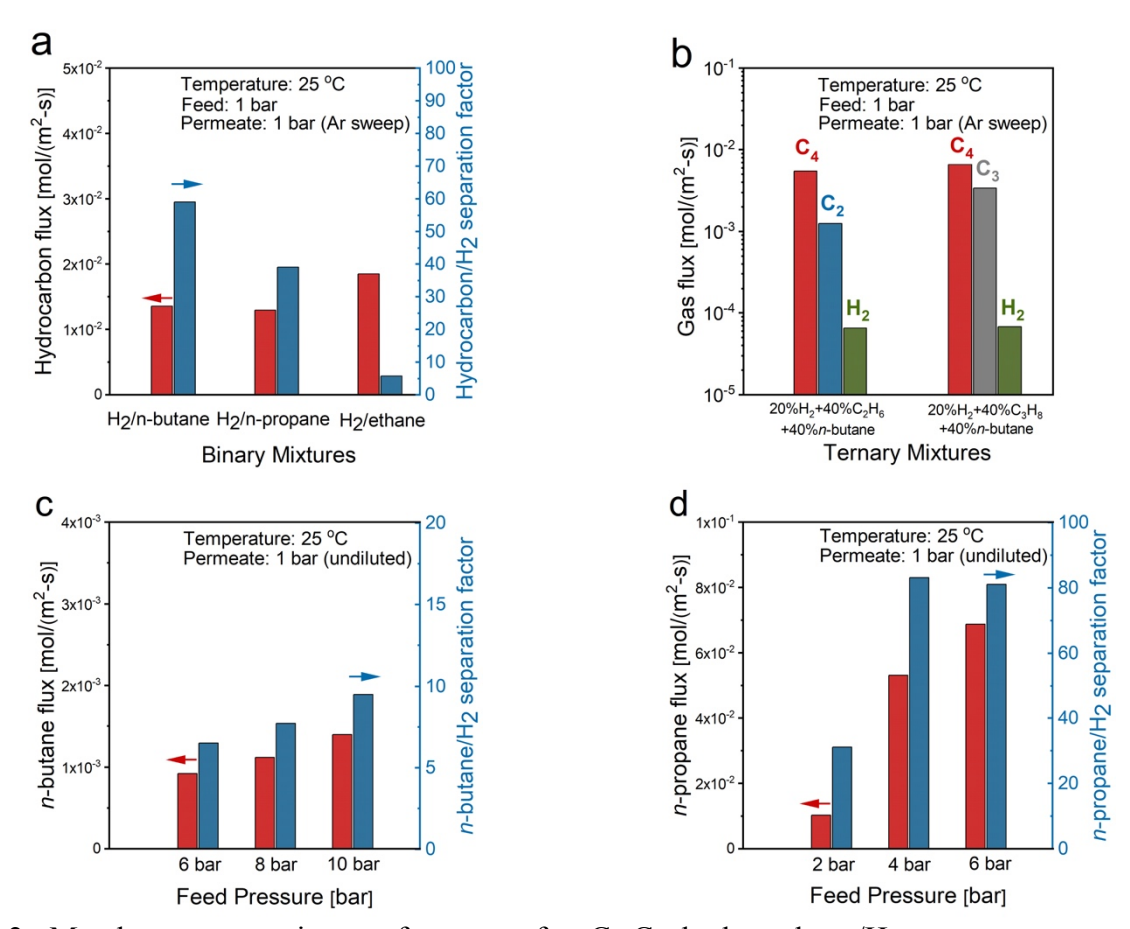


Figure 2. Membrane separation performance for C_2 - C_4 hydrocarbons/ H_2 at room temperature. a) performance for binary H_2 (30%)/various hydrocarbon (70%) (i.e. ethane, n-propane and n-butane) mixtures; b) Flux of components of 20% H_2 -40%ethane-40%n-butane and 20% H_2 -40%n-propane-40%n-butane ternary mixtures; in both a) and b), feed flow rate: 50 mL(STP)/min; feed pressure: 1 bar; sweep (argon) flow rate: 30 mL(STP)/min; permeate pressure: 1 bar; c) performance for H_2/n -butane mixture with a low n-butane concentration (2 mole%) at higher feed pressures; and d) membrane separation performance of equimolar H_2 and n-propane binary mixture at higher feed pressures; in both c) and d), feed flow rate: 200 mL(STP)/min; permeate pressure: 1 bar; no sweep gas used (pure non-diluted permeate).

Conclusions

Zeolite MFI membranes are fabricated from directly-synthesized nanosheets and tested for NH_3/H_2 , NH_3/N_2 , and $H_2/hydrocarbons$ separations at different temperatures and pressures. The membranes exhibit high separation factors and fluxes for the separation of ammonia and hydrocarbons over hydrogen or nitrogen, based on preferential adsorption. The results indicate promise for these high performance MFI membranes to be used for industrial $NH_3/H_2/N_2$ or hydrocarbon/ H_2 separation applications.

Acknowledgements

The authors extend their appreciation to the Deputyship for Research & Innovation, Ministry of Education in Saudi Arabia for funding this research work through the project number (198). The membrane synthesis aspects of this work were supported by the US National Science Foundation (CBET-1705687).

Reference

- 1 G. P. Pez, R. T. Carlin, D. V. Laciak and J. C. Sorensen, US Pat., 4 761 164, 1988.
- 2 D. V. Laciak, G. P. Pez and P. M. Burban, J. Membr. Sci., 1992, 65, 31-38.
- 3 G. P. Pez and D. V. Laciak, US Pat., 4 762 535, 1988.
- 4 A. Bhown and E. L. Cussler, J. Am. Chem. Soc., 1991, 113, 742-749.
- 5 D. V. Laciak and G. P. Pez, US Pat., 4 758 250, 1988.
- 6 Y. He and E. L. Cussler, J. Membr. Sci., 1992, 68, 43-52.
- 7 S. F. Timashev, A. V. Vorobiev, V. I. Kirichenko, Y. M. Popkov, V. I. Volkov, R. R. Shifrina, A. Y. Lyapunov, A. G. Bondarenko and L. P. Bobrova, *J. Membr. Sci.*, 1991, **59**, 117-131.
- 8 B. Bikson, J. K. Nelson and J. E. Perrin, US Pat., 5 009 678, 1991.
- 9 I. V. Vorotyntsev, P. N. Drozdov and N. V. Karyakin, *Inorg. Mater.*, 2006, 42, 231-235.
- 10 W. A. Phillip, E. Martono, L. Chen, M. A. Hillmyer and E. L. Cussler, *J. Membr. Sci.*, 2009, **337**, 39-46.
- 11 C. Makhloufi, B. Belaissaoui, D. Roizard and E.Favre, Procedia Eng., 2012, 44, 143-146.
- 12 O. Camus, S. Perera, B. Crittenden, Y. C. van Delft, D. F. Meyer, P. PAC Pex, I. Kumakiri, S. Miachon, J.A. Dalmon, S. Tennison, P. Chanaud, E. Groensmit and W. Nobel, *AIChE J.*, 2006, **52**, 2055-2065.
- 13 M. Kanezashi, A. Yamamoto, T. Yoshioka and T. Tsuru, AIChE J., 2010, 56, 1204-1212.
- 14 M. Y. Jeon, D. Kim, P. Kumar, P. S. Lee, N. Rangnekar, P. Bai, M. Shete, B. Elyassi, H. S. Lee, K. Narasimharao, S. N. Basahel, S. Al-Thabaiti, W. Xu, H. J. Cho, E. O. Fetisov, R. Thyagarajan, R. F. DeJaco, W. Fan, K. A. Mkhoyan, J. I. Siepmann and M. Tsapatsis, *Nature*, 2017, **543**, 690–694.
- 15 D. Kim, M. Y. Jeon, B. L. Stottrup and M. Tsapatsis, *Angew. Chem., Int. Ed.*, 2018, **130**, 489–494
- 16I. Matito-Martos, A. Martin-Calvo, C. O. Ania, J. B. Parra, J. M. Vicent-Luna and S. Calero, *Chem. Eng. J.*, 2020, **387**, 124062.
- 17 H. Jobic, H. Ernst, W. Heink, J. Kärger, A. Tuel and M. Bée, *Microporous Mesoporous Mater.*, 1998, **26**, 67-75.
- 18 D. K. Ojha, M. J. Kale, A. V. McCormick, M. Reese, M. Malmali, P. Dauenhauer and E. L. Cussler, *ACS Sustain. Chem. Eng.*, 2019, **7**, 18785-18792.
- 19 W. J. Bakker, F. Kapteijn, J. Poppe and J. A. Moulijn, J. Membr. Sci., 1996, 117, 57-78.
- 20 L. J. P. Van Den Broeke, W. J. W. Bakker, F. Kapteijn and J. A. Moulijn, *AIChE J.*, 1999, **45**, 976–985.
- 21 J. Dong, Y. S. Lin and W. Liu, AIChE J., 2000, 46, 1957–1966.
- 22 L. Yu, M. Grahn, P. Ye and J. Hedlund, J. Membr. Sci., 2017, 524, 428–435.
- 23 R. Dragomirova, M. Stöhr, C. Hecker, U. Lubenau, D. Paschek and S. Wohlrab, *RSC Adv.*, 2014, 4, 59831–59834.
- 24 L. Yu, M. Grahn and J. Hedlund, *J. Membr. Sci.*, 2018, **551**, 254–260.
- 25 B. Min, S. Yang, A. Korde, Y. H. Kwon, C. W. Jones and S. Nair, *Angew. Chem., Int. Ed.*, 2019, **58**, 8201–8205.
- 26 B. Min, S. Yang, A. Korde, C. W. Jones and S. Nair, Adv. Mater. Interfaces, 2020, 7, 2000926.
- 27 B. Min, A. Korde, S. Yang, Y. Kim, C. W. Jones and S. Nair, *AIChE J.*, 2020, e17048.
- 28 W. Zhu, J. M. Van De Graaf, L. J. P. Van Den Broeke, F. Kapteijn and J. A. Moulijn, *Ind. Eng. Chem. Res.*, 1998, **37**, 1934–1942.

Supporting Information

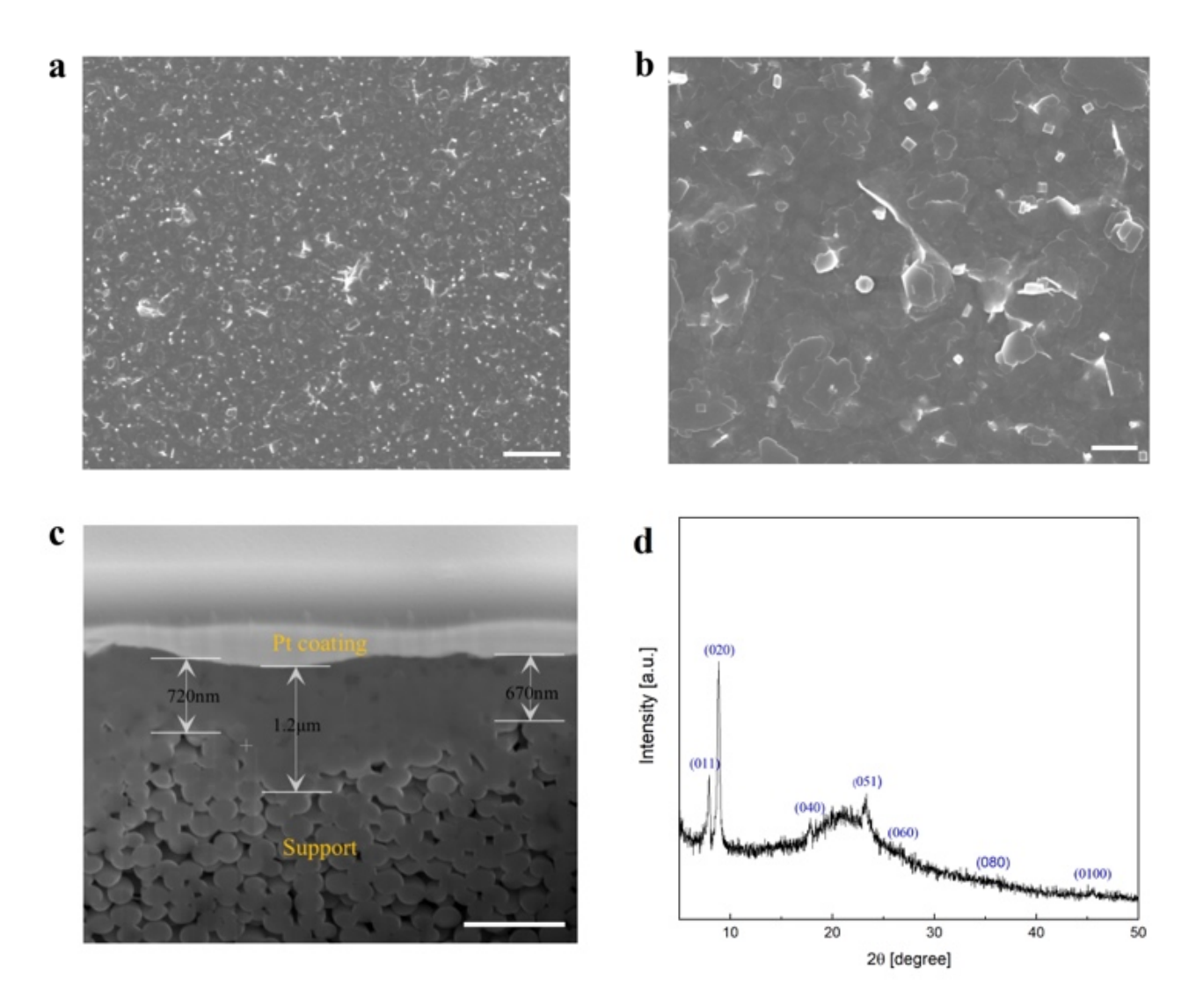


Figure S1: a), b) surface morphology and c) cross-sectional FIB-SEM image of the MFI membrane fabricated from MFI nanosheet seed layer; d) out-of-plane XRD pattern of the fabricated MFI membrane, indicating a dominant b-out-of-plane orientation after secondary growth. The broad background peak is due to the amorphous silica support. Scale bars are a) $5 \mu m$, b) $1 \mu m$, and c) $1 \mu m$.

Table S1: Ammonia/hydrogen binary permeation measurement conditions and membrane performances

			Feed conditions		Pe	ermeate conditio	ns		NH ₃	
ID	Temp	Feed Pressure	Feed composition	Feed flow rate	Permeate pressure	Permeate composition	Permeate flow rate (measured)	NH ₃ flux [mol/(m ² .s)]	permeance (mol/(m².s.Pa))	NH ₃ /H ₂ S.F.
1	25 °C	3 bar	50%H ₂ +50% NH ₃	400 mL/min	1bar (no sweep)	99.62% NH ₃	30.0 mL/min	0.090	2.26×10 ⁻⁶	307
2	50 °C	3 bar	50%H ₂ +50% NH ₃	400 mL/min	1bar (no sweep)	94.9% NH ₃	50.8 mL/min	0.144	3.45×10 ⁻⁶	23.8
3	100 °C	3 bar	50%H ₂ +50% NH ₃	400 mL/min	1bar (no sweep)	75.1% NH ₃	76.6 mL/min	0.173	2.72×10 ⁻⁶	3.8

Sample calculation:

At 25 °C, 3 bar feed pressure, permeate flow rate is 30.0 mL/min.

Converting mL/min to mol/s:

30.0 mL/min =
$$(30.0 \times 10^{-6} \text{ m}^3 \times 101325 \text{ Pa})/(60 \text{ s} \times 8.314 \text{ m}^3 \times \text{Pa} \times \text{K}^{-1} \times \text{mol}^{-1} \times (273.15+25) \text{ K})$$

=2.04×10⁻⁵ mol/s

Effective Membrane Diameter = 1.70 cm

Effective Membrane Area = $3.14 \times (1.70 \times 10^{-2} \text{ m})^2/4 = 0.000227 \text{ m}^2$

NH₃ flux = 2.04×10^{-5} mol/s \times 99.62% /0.000227=0.0895 mol/(m².s)

 $NH_3\ Composition\ in\ Retentate:\ (204\ mL/min-99.62\%\times30.0\ mL/min)/(408\ mL/min-30.0\ mL/min)$

$$=0.461$$

Partial pressure difference = $46.1\% \times 3.01 \times 101325 \text{ Pa} - 99.62\% \times 101325 \text{ Pa} = 39680 \text{ Pa}$

NH₃ permeance = $0.0895 \text{ mol/(m}^2.\text{s})/ 39680 \text{ Pa} = 2.26 \times 10^{-6} \text{ mol/(m}^2.\text{s}.\text{Pa})$

S.F. = (0.9962/0.0038)/(0.461/0.539) = 307

Estimation of expected NH₃ flux

We assume single component NH_3 transport (i.e., neglect the presence of N_2 and H_2 in the membrane) through a membrane and use the following equation to find the flux:

$$J = \frac{\varepsilon Dq_s}{L} \ln(\frac{1 + bP_{feed}}{1 + bP_{nermeate}}) \text{ (ref. }^{S5})$$

Where J is the flux (mol/(m².s)); ε is the support porosity; D is the diffusion coefficient (m²/s); q_s is the saturation loading in mol/m³; L is the membrane thickness and b is the Langmuir parameter.

We use the following parameters:

$$\varepsilon = 0.3$$
:

 $D = 6 \times 10^{-11}$ to 1×10^{-9} m²/s (obtained from Figure 5 of Jobic et al. ^{S6});

 q_s =4.3 mol/kg (estimated from the data of Figure 6 in ref. ^{S7});

The density of MFI zeolite is 1,800 kg/m³;

$$L = 1 \mu m = 1 \times 10^{-6} m;$$

 $b = 8.0 \times 10^{-6} \text{ Pa}^{-1}$ (estimated from the data of Figure 6 in ref. S7);

$$P_{feed} = 1.5 \text{ bar};$$

$$P_{permeate} = 1 \text{ bar.}$$

$$D = 6 \times 10^{-11} \text{ m}^2/\text{s} : J = \frac{0.3 \times 6 \times 10^{-11} \times 4.3 \times 1800}{1 \times 10^{-6}} \ln(\frac{1 + 8.0 \times 10^{-6} \times 1.5 \times 10^5}{1 + 8.0 \times 10^{-6} \times 1.0 \times 10^5}) = 0.028$$

$$D = 1 \times 10^{-9} \text{ m}^2/\text{s} : J = \frac{0.3 \times 1 \times 10^{-9} \times 4.3 \times 1800}{1 \times 10^{-6}} \ln(\frac{1 + 8.0 \times 10^{-6} \times 1.5 \times 10^5}{1 + 8.0 \times 10^{-6} \times 1.0 \times 10^5}) = 0.466$$

Table S2: Ammonia/nitrogen binary permeation measurement conditions and membrane performances

			Feed conditions		Pe	rmeate condition	18		NH ₃	
ID	Temp	Feed Pressure	Feed composition	Feed flow rate	Permeate pressure	Permeate composition	Permeate flow rate (measured)	NH ₃ flux [mol/(m ² .s)]	permeance (mol/(m².s.Pa))	NH ₃ /N ₂ S.F.
1	25 °C	3 bar	50%N ₂ +50%	400	1bar	99.95%	22.0	0.066	1.10×10 ⁻⁶	2236
			NH ₃	mL/min	(no sweep)	NH ₃	mL/min			
2	50 °C	3 bar	50%N ₂ +50%	400	1bar	99.3%	44.5	0.133	2.62×10 ⁻⁶	191
	30 C	3 041	NH_3	mL/min	(no sweep)	NH ₃	mL/min	0.155	2.02710	171
3	50 °C	5 bar	50%N ₂ +50%	400	1bar	99.3%	72.5	0.216	1.89×10 ⁻⁶	219
3	30 C	3 bai	NH_3	mL/min	(no sweep)	NH_3	mL/min	0.216	1.89×10	219
4	50 °C	7 bar	50%N ₂ +50%	400	1bar	99.2%	87.7	0.261	1.66×10 ⁻⁶	221
4	30 C	/ bai	NH_3	mL/min	(no sweep)	NH_3	mL/min	0.201	1.00×10	221
5	100 °C	3 bar	50%N ₂ +50%	400	1bar	92.7%	46.8	0.131	3.47×10 ⁻⁶	15.8
3	100 C	3 0ai	NH_3	mL/min	(no sweep)	NH_3	mL/min	0.131	3.4/X10	13.8
	100 °C	£ 1	50%N ₂ +50%	400	1bar	92.5%	89.4	0.248	2.50×10 ⁻⁶	20.0
6	100 °C	5 bar	NH ₃	mL/min	(no sweep)	NH ₃	mL/min	0.248	2.50×10	20.0

Table S3: H₂/Hydrocarbon binary permeation measurement conditions and membrane performances

			Feed conditions			Permeate condition	ons	Hydrocarbon	Hydrocarbon	Hydrocarbon/
ID	Temp	Feed Pressure	Feed composition	Feed flow rate	Permeate pressure	Permeate composition	Sweep/permeate flow rate	flux [mol/(m².s)]	permeance (mol/(m².s.Pa))	H ₂ S.F.
1	25 °C	1 bar	30%H ₂ +70% <i>n</i> -butane	50 mL/min	1 bar (Ar sweep)	0.083%H ₂ +13.5% <i>n</i> -butane, Ar balance	30 mL/min	0.0135	2.17×10 ⁻⁷	59
2	25 °C	1 bar	30%H ₂ +70% <i>n</i> -propane	50 mL/min	1 bar (Ar sweep)	0.18%H ₂ +15.2% <i>n</i> - propane, Ar balance	30 mL/min	0.0129	2.20×10 ⁻⁷	39
3	25 °C	1 bar	30%H ₂ +70% ethane	50 mL/min	1 bar (Ar sweep)	1.0%H ₂ +20.7% ethane, Ar balance	30 mL/min	0.0184	3.0×10 ⁻⁷	5.7
4	25 °C	6 bar	98%H ₂ +2% <i>n</i> -butane	200 mL/min	1bar (no sweep)	90.5%H ₂ +9.5% <i>n</i> -butane	2.9 mL/min	9.2×10 ⁻⁴	5.8×10 ⁻⁷	6.5
5	25 °C	8 bar	98%H ₂ +2% <i>n</i> -butane	200 mL/min	1bar (no sweep)	86.8%H ₂ +13.2% <i>n</i> -butane	3.1 mL/min	0.0011	5.0×10 ⁻⁷	7.7
6	25 °C	10 bar	98%H ₂ +2% <i>n</i> -butane	200 mL/min	1bar (no sweep)	84.5%H ₂ +15.5% <i>n</i> -butane	3.2 mL/min	0.0014	4.3×10 ⁻⁷	9.5
7	25 °C	2 bar	50%H ₂ +50% <i>n</i> -propane	200 mL/min	1bar (no sweep)	3.3%H ₂ +96.7% <i>n</i> -propane	4.1 mL/min	0.0103	5.3×10 ⁻⁷	31
8	25 °C	4 bar	50%H ₂ +50% <i>n</i> -propane	200 mL/min	1bar (no sweep)	1.5%H ₂ +98.5% <i>n</i> -propane	20.5 mL/min	0.0531	6.3×10 ⁻⁷	83
9	25 °C	6 bar	50%H ₂ +50% <i>n</i> -propane	200 mL/min	1bar (no sweep)	2.2%H ₂ +97.8% <i>n</i> -propane	26.5 mL/min	0.0688	5.9×10 ⁻⁷	81

Table S4: H₂/Hydrocarbon ternary permeation measurement conditions and membrane performances

			Feed conditions		Pe	rmeate condition	ns	<i>n-</i> butane	Ethane/	Hydrogen	<i>n</i> -butane	Ethane
ID	Temp	Feed Pressure	Feed composition	Feed flow rate	Permeate pressure	Permeate composition	Sweep flow rate	flux/permeance	n- propane flux/permeance	flux/permeance	/H ₂ S.F.	or <i>n</i> -propane /H ₂ S.F.
1	25 °C	1 bar	20%H ₂ +40% ethane+40% <i>n</i> -butane	50 mL/min	1 bar (Ar sweep)	0.084%H ₂ +1.6% ethane +7.0% n-butane, Ar balance	30 mL/min	5.50×10^{-3} $mol/(m^2.s)$ 1.65×10^{-7} $mol/(m^2.s.Pa)$	1.26×10 ⁻³ mol/(m ² .s) 3.2×10 ⁻⁸ mol/(m ² .s.Pa)	6.57×10^{-5} mol/(m ² .s) 3.25×10^{-9} mol/(m ² .s.Pa)	42	10
2	25 °C	1 bar	20%H ₂ +40% <i>n</i> -propane+40% <i>n</i> -butane	50 mL/min	1 bar (Ar sweep)	0.084%H ₂ +4.2% n-propane +8.1% n-butane, Ar balance	30 mL/min	6.64×10 ⁻³ mol/(m ² .s) 1.9×10 ⁻⁷ mol/(m ² .s.Pa)	3.41×10 ⁻³ mol/(m ² .s) 1.0×10 ⁻⁷ mol/(m ² .s.Pa)	6.83×10 ⁻⁵ mol/(m ² .s) 3.16×10 ⁻⁹ mol/(m ² .s.Pa)	50	29

Appendix S1: Ammonia separation based on liquid membranes

Ref.	Material	Membrane Thickness	Feed	Sweep	T/°C	NH ₃ permeability /permeance	NH ₃ permeance [mol/(m ² .s.Pa)]	NH ₃ flux (mol/(m ² .s))	NH ₃ /H ₂ selectivity /S.F.	NH ₃ /N ₂ selectivity /S.F.
			1 1							
	Lithium Nitrate		1 bar 10% NH ₃			9900 Barrer				245
	Immobilized Molten Salt		1 bar 25% NH ₃	He, 1 bar	279	7400 Barrer				129
	Membrane		1 bar 50% NH ₃			7100 Barrer				80
			1 bar 10% NH ₃			100,000 Barrer				>1000
			1 bar 20% NH ₃	He,	250	69,000 Barrer				>1000
			1 bar 40% NH ₃	1 bar	230	28,000 Barrer				>1000
			1 bar 80% NH ₃			21,000 Barrer				>1000
[S8] Pez, 1988			1 bar 10% NH ₃			130,000 Barrer				>1000
[S9] Pez, 1992	Zinc Chloride		1 bar 20% NH ₃			79,000 Barrer				>1000
	Immobilized Molten Salt		1 bar 40% NH ₃	He, 1 bar	300	44,000 Barrer				>1000
	Membrane		1 bar 60% NH ₃			43,000 Barrer				>1000
			1 bar 80% NH ₃			33,000 Barrer				>1000
			1 bar 10% NH ₃			140,000 Barrer				>1000
			1 bar 20% NH ₃	He, 1 bar	350	150,000 Barrer				>1000
			1 bar 40% NH ₃			46,000 Barrer				>1000
			1 bar single gas	He, 1 bar	311	290,000 Barrer			3200	
							<u> </u>			
	NH ₃ -				0	2400 GPU	8.0×10 ⁻⁷	0.14		>1000
[S10] Pez,	NH ₃ - NH ₄ SCN Liquid		1NH ₃ :1N ₂	Не	23	1900 GPU	6.36×10 ⁻⁷	0.11		8700
1988	Membrane on Nylon filter		3.6 bar	3.6 bar	21	5265.5 Barrer			59.2	135
					50	5038.6 Barrer			25.8	59.1

Appendix S2: Ammonia separation based on polymeric membranes

Ref.	Material	Membrane Thickness	Feed	Sweep	T/°C	NH ₃ permeance	NH ₃ permeance [mol/(m ² .s.Pa)]	NH ₃ flux [mol/(m ² .s)]	NH ₃ /H ₂ selectivity	NH ₃ /N ₂ selectivity
[S11]	Multi- component		g: 1	11	25	376 GPU	1.26×10 ⁻⁷	0.043	78.8	1423
Kulprathi panja,	silicone rubber/poly	NA	Single gas, 50	1bar, no	25	164 GPU	0.55×10 ⁻⁷	0.019	80.7	1350
1986	ethylene glycol		psig	sweep	25	224 GPU	0.75×10 ⁻⁷	0.026	78.6	1100

Ref.	Material	Membrane Thickness	Feed	Sweep	T/°C	NH ₃ permeance	NH ₃ permeance [mol/(m ² .s.Pa)]	NH ₃ flux (mol/(m ² .s))	NH ₃ /H ₂ selectivity	NH ₃ /N ₂ selectivity
					23.5	118 GPU	0.39×10 ⁻⁷		12.5	450.4
[S12] Pan,	Polysulfone	NA	Single		0	135 GPU	0.45×10 ⁻⁷		33.6	892.8
1988	amide		gas		-10	520 GPU	1.7×10 ⁻⁷		200.8	6025
					-16	1010 GPU	3.4×10 ⁻⁷		653.7	18878

Ref.	Material	Membrane Thickness	Feed	Sweep	T/°C	NH ₃ permeance (GPU)	NH ₃ permeance [mol/(m ² .s.Pa)]	NH ₃ flux [mol/(m ² .s)]	NH ₃ /H ₂ S.F.	NH ₃ /N ₂ S.F.
			3NH ₃ :1N ₂ 1 bar	He, 1 bar	17	2.9 GPU	9.7×10 ⁻¹⁰	0.000073		>50
		80-150 μm	3NH ₃ :1N ₂ 5 bar	He, 5 bar	17	16 GPU	5.4×10 ⁻⁹	0.0020		>800
	Polyvinyl- ammonium		3NH ₃ :1N ₂ 6 bar	He, 6 bar	17	50 GPU	1.7×10 ⁻⁸	0.0090		>1000
	chloride		60% NH ₃ 13.8 bar	He, 1 bar	25	32 GPU	1.1×10 ⁻⁸	0.0089		2100
		~180 µm	40% NH ₃ 20.7 bar	He, 1 bar	25	27 GPU	9.0×10 ⁻⁹	0.0075		2500
			30% NH ₃ 27.5 bar	He, 1 bar	25	24 GPU	8.0×10 ⁻⁹	0.0066		2200
			3NH ₃ :1N ₂ 1 bar	He, 1 bar	17	98 GPU	3.3×10 ⁻⁸	0.0025		>900
			3NH ₃ :1N ₂ 6 bar	He, 6 bar	17	250 GPU	8.4×10 ⁻⁸	0.038		>1100
		NA	3NH ₃ :1N ₂ 3 bar	He, 3 bar	52	150 GPU	5.0×10 ⁻⁸	0.011		>1000
		NA	3NH ₃ :1N ₂ 6 bar	He, 6 bar	52	220 GPU	7.4×10 ⁻⁸	0.033		>1100
[S13] Pez,			3NH ₃ :1N ₂ 3 bar	He, 3 bar	73	110 GPU	3.7×10 ⁻⁸	0.0083		>900
1988			3NH ₃ :1N ₂ 6 bar	He, 6 bar	73	160 GPU	5.4×10 ⁻⁸	0.024		>1000
			38.8% NH ₃ 20.5 bar	He, 1 bar	26	340 GPU	1.1×10 ⁻⁷	0.090		1500
	Polyvinylam monium		28.6% NH ₃ 27.8 bar	He, 1 bar	26	230 GPU	7.7×10 ⁻⁸	0.061		1300
	thiocyanate	100-300	25.4% NH ₃ 31.2 bar	He, 1 bar	26	210 GPU	7.0×10 ⁻⁸	0.056		1200
		μm	18.6% NH ₃ 42.7 bar	He, 1 bar	26	150 GPU	5.0×10 ⁻⁸	0.040		1100
			13.4% NH ₃ 59.2 bar	He, 1 bar	26	110 GPU	3.7×10 ⁻⁸	0.022		970
			12.0% NH ₃ 66.4 bar	He, 1 bar	26	97 GPU	3.2×10 ⁻⁸	0.026		890
			13.8% NH ₃ +25.9%H ₂ +60.3%N ₂ 57.5 bar	He, 1 bar	24	54 GPU	1.8×10 ⁻⁸	0.014	6200	3600
			13.8% NH ₃ +25.9%H ₂ +60.3%N ₂ 57.5 bar	He, 1 bar	60	32 GPU	1.1×10 ⁻⁸	0.0085	1400	2000

Ref.	Material	Membrane Thickness	Feed	Sweep	T/°C	NH ₃ permeance	NH ₃ permeance [mol/(m ² .s.Pa)]	NH ₃ flux [mol/(m ² .s)]	NH ₃ /H ₂ S.F.	NH ₃ /N ₂ S.F.
[010]	Polyvinyl-		13.111		0	183 GPU	6.1×10 ⁻⁸	0.011		>3000
[S10] Pez, 1988	alcohol ammonium	~200 µm	1NH ₃ : 1N ₂ 3.6 bar	He 3.6 bar	19	179 GPU	6.0×10 ⁻⁸	0.011		3000
1988	thiocyanate		3.0 0ai		50	180 GPU	6.0×10 ⁻⁸	0.011		1000

Ref.	Material	Membrane Thickness	Feed	Sweep	T/°C	NH ₃ permeance	NH ₃ permeance [mol/(m ² .s.Pa)]	NH ₃ flux [mol/(m ² .s)]	NH ₃ /H ₂ selectivity	NH ₃ /N ₂ selectivity
[S14] Timashev, 1991	Hydrolyzed Perfluosro- sulfonic acid polymer hollow fibers	Wall thickness 17 µm	Single gas, 2bar	He, 1 bar	25	459 GPU	1.54×10 ⁻⁷	0.031	> 100-1000	

Ref.	Material	Membrane Thickness	Feed	Sweep	T/ °C	NH ₃ permeance	NH ₃ permeance [mol/(m².s.Pa)]	NH ₃ flux [mol/(m ² .s)]	NH ₃ /H ₂ S.F.	NH ₃ /N ₂ S.F.
[S15]	Composite polysulfone		NH ₃ /N ₂ /H ₂		22	132.6 GPU	4.4×10 ⁻⁸	0.0031	33	>1000
Bikson, 1991	hollow fiber/ sulfonated polysulfone		10/30/60 100 psig		9	157.3 GPU	5.3×10 ⁻⁸	0.0036	63	>1000

Ref.	Material	Membrane Thickness	Feed	Sweep	T/° C	NH ₃ permeance	NH ₃ permeance [mol/(m ² .s.Pa)]	NH ₃ flux [mol/(m ² .s)]	NH ₃ /H ₂ selectivity /S.F.	NH ₃ /N ₂ selectivity /S.F.
[S16] Cussler, 1992	Perfluoro- sulfone (Nafion) Different ionic forms	38 μm	5.4 bar NH ₃ /N ₂ mixture, ratio not given.	Не	21 200			0.14 0.10 0.084 0.070 0.040 0.038 0.035 0.013 0.019 0.012 0.017 0.0087 0.0050 0.0059 0.0061 NA		>3000 >3000 600 600 600 >3000 >3000 >3000 >3000 >3000 >3000 3000 120 60 >3000 60 >3000
[S17] Vorotynt sev, 2006	Cellulose acetate		Single gas, 1bar	<4.1 kPa	25	292 GPU	9.8×10 ⁻⁸	0.0098	9.3	111
[S18] Cussler, 2009	Poly(norbor enylethysty rene)-b- poly(propyl styrene- sulfonate) copolymer	NA	Single gas, 2bar	1 bar	25	>600 Barrer				>90
[S19]	poly[bis(trif				5	5643.7 Barrer			105.3	221.3
Makhlou	luoroethoxy)phosphaze ne]	NA	Single gas	Vacuum	21	5265.5 Barrer			59.2	135
fi,2012	(PTFEP)				50	5038.6 Barrer			25.8	59.1

Appendix S3: Ammonia separation based on silica membranes

Ref.	Material	Membrane Thickness	Feed	Sweep	T/°C	NH ₃ permeance	NH ₃ permeance [mol/(m ² .s.pa)]	NH ₃ flux (mol/(m ² .s))	NH ₃ /H ₂ S.F.	NH ₃ /N ₂ S.F.
[S20] Camus, 2006	Tubular silica membranes on alumina substrates	<200nm	16% NH ₃ , 3/1 H ₂ /N ₂ 10 bar	1 bar	80	2275 GPU	7.62×10^{-7}	0.12	6.60	14.48
			14% NH ₃ , 3/1 H ₂ /N ₂ 16.3 bar	1 bar	80	513 GPU	1.72 × 10 ⁻⁷	0.039	2.74	1.59
			14% NH ₃ , 3/1 H ₂ /N ₂ 21.2 bar	1 bar	80	1107 GPU	3.71 × 10 ⁻⁷	0.11	4.89	7.10
			14% NH ₃ , 3/1 H ₂ /N ₂ 25.2 bar	1 bar	80	1687 GPU	5.65 × 10 ⁻⁷	0.20	4.88	10.73
	Si-1, average		1bar 1/1 NH ₃ /H ₂	1 bar	50	304 GPU	1.02×10^{-7}	0.0051	28.7	
[S21] Kaneza shi, 2010	pore size 0.5-0.6 nm				400	310 GPU	1.04×10^{-7}	0.0052	0.083	
	Si-2, average	<1 μm	1 bar 1/1 NH ₃ /H ₂	1 bar	50	50 GPU	0.168×10^{-7}	0.00084	1.02	
	pore size 0.4-0.5 nm				400	35 GPU	0.117×10^{-7}	0.00058	0.018	
	Si-3, average pore size 0.3 nm		1 bar 1/1 NH ₃ /H ₂	1 bar	50	1.5 GPU	0.00521×10^{-7}	0.000026	0.31	

Appendix S4: Ammonia separation based on MFI membranes

Ref.	Material	Membrane Thickness	Feed	Sweep	T/°C	NH ₃ permeance	NH ₃ permeance [mol/(m ² .s.Pa)]	NH ₃ flux [mol/(m ² .s)]	NH ₃ /H ₂ S.F.	NH ₃ /N ₂ S.F.
[S20] Camus , 2006	MFI on alumina tube	5-15µm	16% NH ₃ , 3/1 H ₂ /N ₂ 10bar	1 bar	80		2.14 × 10 ⁻⁷	0.034	9.13	14.09
			16% NH ₃ , 3/1 H ₂ /N ₂ 10bar	1 bar	25		0.60×10^{-7}	0.0096	2.80	3.10
			9% NH ₃ , 3/1 H ₂ /N ₂ 10bar	1 bar	25		0.64×10^{-7}	0.0058	3.08	2.84
			2% NH ₃ , 3/1 H ₂ /N ₂ 10bar	1 bar	25		0.92×10^{-7}	0.0018	5.00	4.61
	MFI on fiber		16% NH ₃ , 3/1 H ₂ /N ₂ 10bar	1 bar	80		0.13×10^{-7}	0.0021	7.14	20.66

Appendix S5: Literature reports of MFI membranes for sorption-based selective separation

Ref.	Membrane Thickness	Mixture	Sweep	Pressure	T.	Hydrocarbon flux/permeance	S.F.
[S22] Moulijn, 1999	50-60 μm	5 <i>n</i> -C ₄ :95H ₂	Не	1 bar	295 K	1×10 ⁻³ mol/(m ² .s)	125
[S23] Moulijn, 1999	50-60 μm	50n-C ₄ :50H ₂	Yes	1 bar	300 K	5×10 ⁻³ mol/(m ² .s)	40
[S24] Lin, 2000	3-5 μm	84.48H ₂ :7.59CH ₄ :2.51C ₂ H ₆ :2.52C ₂ H ₄ :0.75C ₃ H ₈ :1.45C ₃ H ₆ :0.4 <i>n</i> -C ₄ :0.3i-C ₄	5.6-12.1 mL/min	1 bar	298 K	2-4×10 ⁻⁴ mol/(m ² .s)	H ₂ not detected
	0.5 μm	$20C_3H_6:80N_2$	No	10 bar	298 K	22×10 ⁻⁷ mol/(m ² .s.Pa)	43
[S25] Hedlund, 2017		20C ₂ H ₄ :80N ₂	No	10 bar	277 K	57×10 ⁻⁷ mol/(m ² .s.Pa)	6
[S26]Dragomirova, R. et al, 2014	40 μm	92CH ₄ :8 <i>n</i> -C ₄	vacuum	1bar	298 K	1.36×10 ⁻⁵ mol/(m ² .s)	39
[S27] Hedlund, 2018	0.4 μm	10 <i>n</i> -C4:90CH4	No	9 bar	298 K	$31\times10^{-7} mol/(m^2.s.Pa)$	25
2018		10C ₃ H ₈ :90CH ₄	No	9 bar	297 K	$54 \times 10^{-7} \text{mol/(m}^2.\text{s.Pa})$	9.5
FG20131 : 2010	<0.8 μm	17.5 <i>n</i> -C ₄ :82.5CH ₄	Ar	1 bar	298 K	$8.4 \times 10^{-7} \text{mol/(m}^2.\text{s.Pa})$	300
[S28] Nair, 2019		16.5C ₃ H ₈ :83.5CH ₄	Ar	1 bar	298 K	16.7× 10 ⁻⁷ mol/(m ² .s.Pa)	45
[S29] Nair, 2020	0.3-1.2μm	76CH ₄ :8C ₂ H ₆ :8C ₃ H ₈ :8 <i>n</i> -C ₄ H ₁₀	Ar	9 bar	298 K	n-butane: 460 GPU n-propane: 220 GPU ethane: 31 GPU	n-C ₄ /CH ₄ : 97 C ₃ H ₈ /CH ₄ : 48 C ₂ H ₆ /CH ₄ : 7
		10 <i>n</i> -C ₄ :90CH ₄	Ar	1-10 bar	298 K	800-2500 GPU	125-250
		10n-C ₃ H ₈ :90CH ₄	Ar	1-9 bar	298 K	1500-3200 GPU	15-25
[S30] Nair, 2020	0.8-1 μm	$X''(H) \cdot Qn_{-}(H) \cdot Qn_{-}(H) \cdot H \cdot$		<i>n</i> -butane: 700-2500 GPU <i>n</i> -propane: 100-350 GPU	n-C ₄ /CH ₄ : 150-250 n-C ₃ H ₈ /CH ₄ : 25-40		
		76CH ₄ :8C ₂ H ₆ :8 <i>n</i> -C ₃ H ₈ :8 <i>n</i> -C ₄ H ₁₀	Ar	1-9 bar	298 K	<i>n</i> -butane: 700-2700 GPU <i>n</i> -propane: 175-500 GPU ethane: 15-35 GPU	n-C ₄ /CH ₄ : 160-280 n-C ₃ H ₈ /CH ₄ : 45-60 C ₂ H ₆ /CH ₄ : 4

1GPU=3.35× 10⁻¹⁰mol/(m².s.Pa)

References:

- S1. M. Y. Jeon, D. Kim, P. Kumar, P. S. Lee, N. Rangnekar, P. Bai, M. Shete, B. Elyassi, H. S. Lee, K. Narasimharao, S. N. Basahel, S. Al-Thabaiti, W. Xu, H. J. Cho, E. O. Fetisov, R. Thyagarajan, R. F. DeJaco, W. Fan, K. A. Mkhoyan, J. I. Siepmann and M. Tsapatsis, *Nature*, 2017, **543**, 690–694.
- S2. K. V. Agrawal, B. Topuz, T. C. T. Pham, T. H. Nguyen, N. Sauer, N. Rangnekar, H. Zhang, K. Narasimharao, S. N. Basahel, L. F. Francis, C. W. Macosko, S. Al-Thabaiti, M. Tsapatsis and K. B. Yoon, *Adv. Mater.*, 2015, **27**, 3243–3249.
- S3. T. C. T. Pham, T. H. Nguyen and K. B. Yoon, *Angew. Chem.*, *Int. Ed.*, 2013, **52**, 8693–8698.
- S4. D. Kim, M. Y. Jeon, B. L. Stottrup and M. Tsapatsis, *Angew. Chem., Int. Ed.*, 2018, **130**, 489–494.
- S5. V. Nikolakis, G. Xomeritakis, A. Abibi, M. Dickson, M. Tsapatsis and D. G. Vlachos, *J. Membr. Sci.*, 2001, **184**, 209-219.
- S6. H. Jobic, H. Ernst, W. Heink, J. Kärger, A. Tuel and M. Bée, *Microporous Mesoporous Mater.*, 1998, **26**, 67-75.
- S7. I. Matito-Martos, A. Martin-Calvo, C. O. Ania, J. B. Parra, J. M. Vicent-Luna and S. Calero, *Chem. Eng. J.*, 2020, **387**, 124062.
- S8. G. P. Pez, R. T. Carlin, D. V. Laciak and J. C. Sorensen, US Pat., 4 761 164, 1988.
- S9. D. V. Laciak, G. P. Pez and P. M. Burban, J. Membr. Sci., 1992, 65, 31-38.
- S10. G. P. Pez and D. V. Laciak, US Pat., 4 762 535, 1988.
- S11. S. Kulprathipanja and S. S. Kulkarni, US Pat., 4 608 060, 1986.
- S12. C. Y. Pan and E. M. Hadfield, US Pat., 4 793 829, 1988.
- S13. D. V. Laciak and G. P. Pez, US Pat., 4 758 250, 1988.
- S14. S. F. Timashev, A. V. Vorobiev, V. I. Kirichenko, Y. M. Popkov, V. I. Volkov, R. R. Shifrina, A. Y. Lyapunov, A. G. Bondarenko and L. P. Bobrova, *J. Membr. Sci.*, 1991, **59**, 117-131.
- S15. B. Bikson, J. K. Nelson and J. E. Perrin, US Pat., 5 009 678, 1991.
- S16. Y. He and E. L. Cussler, *J. Membr. Sci.*, 1992, **68**, 43-52.
- S17. I. V. Vorotyntsev, P. N. Drozdov and N. V. Karyakin, *Inorg. Mater.*, 2006, 42, 231-235.
- S18. W. A. Phillip, E. Martono, L. Chen, M. A. Hillmyer and E. L. Cussler, *J. Membr. Sci.*, 2009, **337**, 39-46.
- S19. C. Makhloufi, B. Belaissaoui, D. Roizard and E.Favre, *Procedia Eng.*, 2012, 44, 143-146.
- S20. O. Camus, S. Perera, B. Crittenden, Y. C. van Delft, D. F. Meyer, P. PAC Pex, I. Kumakiri, S. Miachon, J.A. Dalmon, S. Tennison, P. Chanaud, E. Groensmit and W. Nobel, *AIChE J.*, 2006, **52**, 2055-2065.
- S21. M. Kanezashi, A. Yamamoto, T. Yoshioka and T. Tsuru, AIChE J., 2010, 56, 1204-1212.
- S22. W. J. Bakker, F. Kapteijn, J. Poppe and J. A. Moulijn, J. Membr. Sci., 1996, 117, 57-78.
- S23. L. J. P. Van Den Broeke, W. J. W. Bakker, F. Kapteijn and J. A. Moulijn, *AIChE J.*, 1999, **45**, 976–985.
- S24. J. Dong, Y. S. Lin and W. Liu, AIChE J., 2000, 46, 1957–1966.
- S25. L. Yu, M. Grahn, P. Ye and J. Hedlund, J. Membr. Sci., 2017, **524**, 428–435.
- S26. R. Dragomirova, M. Stöhr, C. Hecker, U. Lubenau, D. Paschek and S. Wohlrab, *RSC Adv.*, 2014, **4**, 59831–59834.
- S27. L. Yu, M. Grahn and J. Hedlund, J. Membr. Sci., 2018, 551, 254–260.
- S28. B. Min, S. Yang, A. Korde, Y. H. Kwon, C. W. Jones and S. Nair, *Angew. Chem., Int. Ed.*, 2019, **58**, 8201–8205.
- S29. B. Min, S. Yang, A. Korde, C. W. Jones and S. Nair, *Adv. Mater. Interfaces*, 2020, 7, 2000926.
- S30. B. Min, A. Korde, S. Yang, Y. Kim, C. W. Jones and S. Nair, *AIChE J.*, 2020, e17048.